ADVANCED FUNCTIONAL MATERIALS
www.afm-journal.de

Bifunctional Piezo-Enhanced PLLA/ZA Coating Prevents Aseptic Loosening of Bone Implants

Xi Cui, Yizhu Shan, Jiaxuan Li, Meng Xiao, Yuan Xi, Jianying Ji, Engui Wang, Baokun Zhang, Lingling Xu, Mingzhu Zhang,* Zhou Li,* and Yingzi Zhang**

Prevention of aseptic loosening, the main reason for secondary surgery of bone implants, is of great crucial clinical importance. As a promising bioactive material to promote bone regeneration, the piezoelectric materials for preventing aseptic loosening has not been reported. Here, a surface coating is presented for implants based on piezoelectric poly(L-lactic acid) (PLLA). The coating ingeniously utilizes zoledronic acid (ZA), a drug used to treat osteoporosis, as a nucleating agent to enhance the piezoelectricity of PLLA. The coating can not only provide a continuous porous piezoelectric environment to stimulate osteogenic differentiation without intervention, but also effectively inhibit the osteolytic activity of osteoclasts through the slow release of ZA, achieving long-term effectiveness with a single implantation. The rat femur cavity implantation experiment suggests that, the PLLA/ZA coating can rapidly initiate osseointegration of the implant and effectively mitigate the risk of aseptic loosening, even in the presence of metal submicroscopic particles that induce aseptic loosening. This strategy of piezo-enhanced PLLA drug-loaded coating may provide a new idea for the surface modification of bone implants.

1. Introduction

Arthroplasty, anticipated 1.9 million total hip and knee replacements will be performed annually in the United States by 2030,[1] is a common surgical intervention in orthopaedics.[1] However, more than 10% of these procedures require further revision due to aseptic loosening, resulting in increased financial losses and patient suffering.[2,3] Aseptic loosening is usually thought to be a loosening of the joint prosthesis caused by abnormal phagocytosis by macrophages due to microscopic particles generated by wear and tear of the bone implant. Abnormal osteolysis by osteoclasts at the implant and bone interface leads to increased loosening, which in turn produces more wear particles, creating a vicious cycle.[4,5] To break this cycle, it is crucial to inhibit inflammation and promote rapid osseointegration at the implant-bone interface.[6,7]

Surface modification of bone implants is the main method to promote osseointegration.[8] Researchers have used titanium dioxide nanotubes,[9–11] polymers,[12–14] and hydroxyapatite[15,16] as carriers to load various drugs. In addition, different methods such as layer self-assembly technology, bionic co-deposition and physical adsorption have been proposed to combine it with the implant to form a functional coating.[17,18] On the one hand, the carrier material can change the morphology, structure, and chemical properties of the surface of the bone implant, and on the other hand, the effective loading and controlled release of drugs can be realized to promote osseointegration.[13] Recently, more and more biomaterials

X. Cui, Y. Shan, J. Li, M. Xiao, Y. Xi, J. Ji, E. Wang, B. Zhang, L. Xu, Z. Li
Beijing Key Laboratory of Micro-nano Energy and Sensor
Beijing Institute of Nanoenergy and Nanosystems
Chinese Academy of Sciences
Beijing 101400, China
E-mail: xull2021@nanoctr.cn; zli@binn.cas.cn

X. Cui, Y. Shan, J. Li, Z. Li
School of Nanoscience and Engineering
University of Chinese Academy of Sciences
Beijing 100049, China

Y. Shan, Y. Zhang
Department of Orthopedics
The Second Affiliated Hospital of Soochow University
No. 1055, Sanxiang Road, Gusu District, Suzhou, Jiangsu 215004, China
E-mail: zhangyz@suda.edu.cn

L. Xu
New Cornerstone Science Laboratory
CAS Key Laboratory for Biomedical Effects of Nanomaterials and Nanosafety and CAS Center for Excellence in Nanoscience
National Center for Nanoscience and Technology
Beijing 100190, China

M. Zhang
Department of Foot and Ankle Surgery, Beijing Tongren Hospital
Capital Medical University
Beijing 100730, China
E-mail: mingzhuzhang@mail.ccmu.edu.cn

The ORCID identification number(s) for the author(s) of this article can be found under https://doi.org/10.1002/adfm.202403759

DOI: 10.1002/adfm.202403759

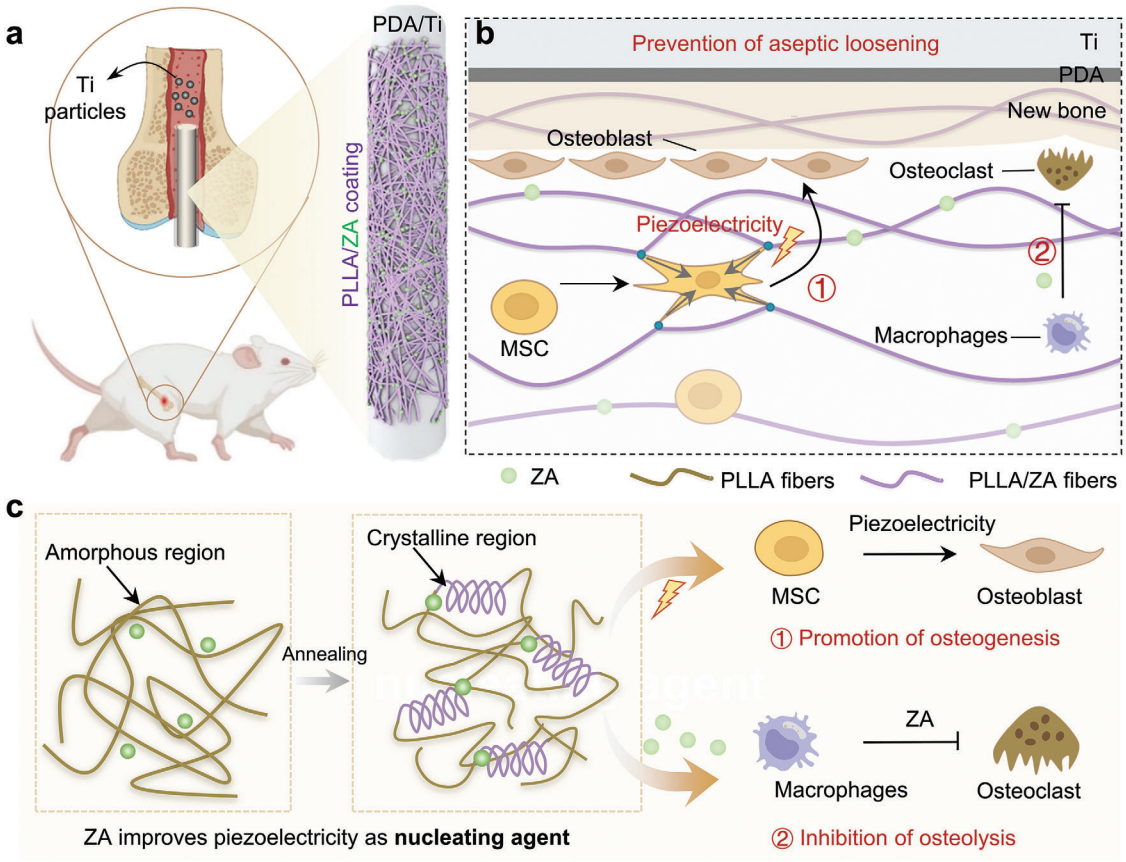

Figure 1. Biological effects of PLLA/ZA coating to prevent aseptic loosening of implants. a) A PLLA/ZA-coated titanium rod (modified with a PDA layer between them) implanted in the femoral cavity of rat, and titanium particles were injected into the bone cavity to simulate the release of particles caused by wear. b) MSCs adhered to the surface of PLLA/ZA fibers via integrins, and then the fibers were deformed by cell traction force, which caused piezoelectricity to promote the differentiation of MSCs into osteoblasts. c) ZA can act as nucleating agent to promote the crystallinity of PLLA and thus enhance the piezoelectricity, but also act as an anti-osteoporosis drug to inhibit the differentiation of macrophages into osteoclasts.

and strategies have been developed to modify implants. However, these expensive, complicated, and single-purpose coatings do not yet meet the clinical requirements for improved outcomes.[8,19,20] Therefore, it is necessary to find an alternative approach that can accelerate osseointegration effectively.

In this aspect, electrical stimulation therapy has been proved to be an effective means to promote bone repair.[21,22] Conventional power sources for electrical stimulation are the external power supply, while piezoelectric materials provide a new idea as self-powered system in bone tissue engineering with its unique power conversion ability.[23–25] Currently, piezoelectric materials have shown promising repair effects in fractures, large bone defects, and osteoarthritis.[26–28] The surface modification of bone implants with piezoelectric materials is expected to enhance osteogenic differentiation and achieve rapid bone integration through the introduction of electrical stimulation, which has not been reported yet. As a biocompatible and degradable piezoelectric material, poly(L-lactic acid) (PLLA) has great application potential for implants. However, the low piezoelectric coefficient requires organismal motion or the appliying of ultrasound to generate effective electrical signals.[29,30] Motion may lead to further wear of bone implants, and external ultrasound intervention has shortcoming such as poor patient compliance. Therefore, improving the piezoelectricity of PLLA is a simpler and more effective method. In this way, the traction force during cell growth and migration can cause much higher piezoelectric signals to activate cells.[31,32] The piezoelectricity of PLLA is directly related to its crystallinity, adding nucleating agents to increase the crystallinity of PLLA is an effective way to improve its piezoelectricity.[33,34] In addition, with the mechanism of aseptic loosening, selecting drugs with anti-inflammatory and inhibitory osteoclastic activity as nucleating agents can make the coating have the double functions at the same time, so as to achieve the purpose of synergistic treatment.[16,35]

In this study, we prepared a zoledronic acid (ZA)-loaded PLLA piezoelectric spinning coating (PLLA/ZA) on the Ti metal surface, in which ZA was a commonly used osteoporosis drug, as the nucleating agent of the crystallization process of PLLA. Polydopamine (PDA) was modified on the Ti surface as an adhesion layer to ensure a tight binding of the spun layer.[36] Ti particles were injected into the femoral bone cavity to simulate the wear particles after the occurrence of aseptic loosening (**Figure 1a**).[37] Importantly, ZA plays two roles in the coating. ZA increased the piezoelectricity of PLLA to promote osteogenic differentiation, and on the other hand, slow-releasing ZA directly inhibited osteoblast differentiation and osteolysis,

achieving rapid osseointegration of the implant and breaking the vicious cycle of further dislodgement and shedding of wear particles (Figure 1b). Figure 1c demonstrates the crystallization process of PLLA, where the amorphous regions of PLLA with ZA as the nucleus were transformed into crystalline regions during the annealing process. Overall, the strategy of ZA as a nucleating agent to improve the piezoelectricity of PLLA not only eliminates the trouble of externally applied interventions, but also ZA realizes targeted prevention and treatment in clinical application scenarios for the processing of bone implants.

2. Results and Discussions

2.1. Preparation and Characterization of PLLA/ZA Piezoelectric Coating

The piezoelectric coatings were obtained through a process of electrostatic spinning on the Ti surface, during which PDA was first modified on the Ti surface to improve the adhesion between the spinning layer and Ti. Ti rods with a diameter of 1 mm were used for in vivo experiments and Ti sheets with a diameter of 14 mm were used for in vitro experiments. The optical photographs of the prepared implants are shown in **Figure** 2a. After modification by PDA, the Ti surface changed from silver to dark brown, indicating uniform polymerization of PDA on the Ti surface. Futhermore, the spinning coating adhered tightly to it. The bond strength of the spinning layer to the Ti sheet was increased from 0.14 N to 1.73 N compared to the Ti sheet without PDA modification (Figure 2b,c).

According to the results of scanning electron microscope (SEM) and field emission scanning electron microscope energy spectrometer (EDS) analysis of the PLLA/ZA coating on the surface of the Ti rods, the distribution of N and P elements showed that ZA was uniformly distributed in the PLLA fiber layer (Figure 2d). The thickness of the coating was ≈ 50 µm (Figure 2e). The addition of ZA did not affect the morphology of the fibers compared to the PLLA fibers alone (Figure S1, Supporting Information). The fiber diameters were around 1 µm, with a loose distribution among them (Figure 2f).

To verify the effect of ZA on the piezoelectricity of PLLA, we examined the crystallinity, differential thermal scanning calorimetry (DSC) curves and piezoelectricity in the d_{14} direction of PLLA and PLLA/ZA spun films.[38] The X-Ray diffraction (XRD) spectra showed distinct diffraction peaks at 16.9° (110/200, α-phase) for PLLA and PLLA/ZA, with the full width at half maximum (FWHM) of the diffraction peaks for PLLA/ZA being much smaller than that of PLLA, suggesting a higher crystallinity (Figure 2g). Based on the crystallization and melting peaks from the DSC curves, we calculated that the crystallinity of PLLA is 21.65%, while the crystallinity of PLLA/ZA is 37.89% (Figure 2h).[39] Furthermore, the piezoelectricity of the spun films in the d_{14} direction was tested using our laboratory's own platform, and the piezoelectric coefficient of PLLA/ZA was 8.02 pC/N, which is much higher than that of PLLA (2.24 pC/N) (Figure 2i).

To test the degradability of the PLLA/ZA coatings, we performed accelerated degradation experiments on them in phosphate buffered saline (PBS) at 60 °C. The experimental results showed that the film started to crack after 2 weeks and almost completely broke into small fragments after 8 weeks (Figure 2j), and the quality of the film gradually decreased with time (Figure 2k). As shown in Figure 2l, the concentration of P, a characteristic element of ZA, was tested and the amount of P dissolved in deionized water gradually increased with time at 37 °C, indicating that ZA can be released slowly in the body.

2.2. Biocompatibility of PLLA/ZA Coating

For in vitro cellular experiments, titanium plates were used for surface modification, as shown in **Figure** 3a. The titanium plates were immersed in a solution containing dopamine to form a uniform PDA coating, and then PLLA coatings were further prepared by high-voltage electrospinning and directional arranged fibers could be obtained by using a high-speed rotating receiver. Primary mesenchymal stem cells (MSCs), as the precursor cells of osteogenesis, were used to test the cytocompatibility of the spinning coatings. Ti sheets were used as a control, and to assess the effect of piezoelectricity, the unannealed PLLA is named PLA, is virtually devoid of piezoelectric output. Cells grown on Ti, PLA, PLLA and PLLA/ZA surfaces for 24 hours and stained by live/dead assays, which showed that there was no significant difference in all groups, consisting mainly of green living cells and almost no red dead cells. (Figure 3b; Figure S2, Supporting Information). Figure 3c shows that MSCs grew for 48 h on the surface of spun fibers, compared to the Ti surface, grew along the direction of the fibers, with the highest number of cells in the PLLA/ZA group (Figure S3, Supporting Information), which correlates with piezoelectricity-enhanced cell proliferation. Cell counting Kit-8 (CCK8) assay showed that the cells proliferated significantly with the prolongation of culture time, and the absorbance of PLLA/ZA group was significantly higher than that of control group (Figure 3d). The above results indicate that MSCs can adhere, grow, and orient themselves on the piezoelectric coating surface, and the piezoelectric material also has the ability to promote MSCs proliferation.

In order to investigate the blood compatibility of the materials, the hemolysis rate and platelet activation ability of the materials were characterized. Using deionized water as a positive control and PBS as a negative control, the PLA, PLLA, and PLLA/ZA materials showed a haemolysis rate of less than 5%, indicating that the materials were not hemolytic (Figure 3e,f). In the platelet activation assays, there was no significant difference in the ability of the material to activate platelets compared with control group (Figure 3g,h). The above results indicate that the material had good blood compatibility.

2.3. The Effect of Piezoelectricity of PLLA/ZA on Osteogenic Differentiation

The nN-level cell traction force generated during cell growth and migration can deform ZnO nanosheets,[40] PVDF piezoelectric fibers,[41] and PLLA piezoelectric fibers[32] to produce piezoelectric signals. In this study, MSCs deform the fibers during growth and migration, thereby generating piezoelectric signals that can accelerate the osteogenic differentiation of MSCs and promote

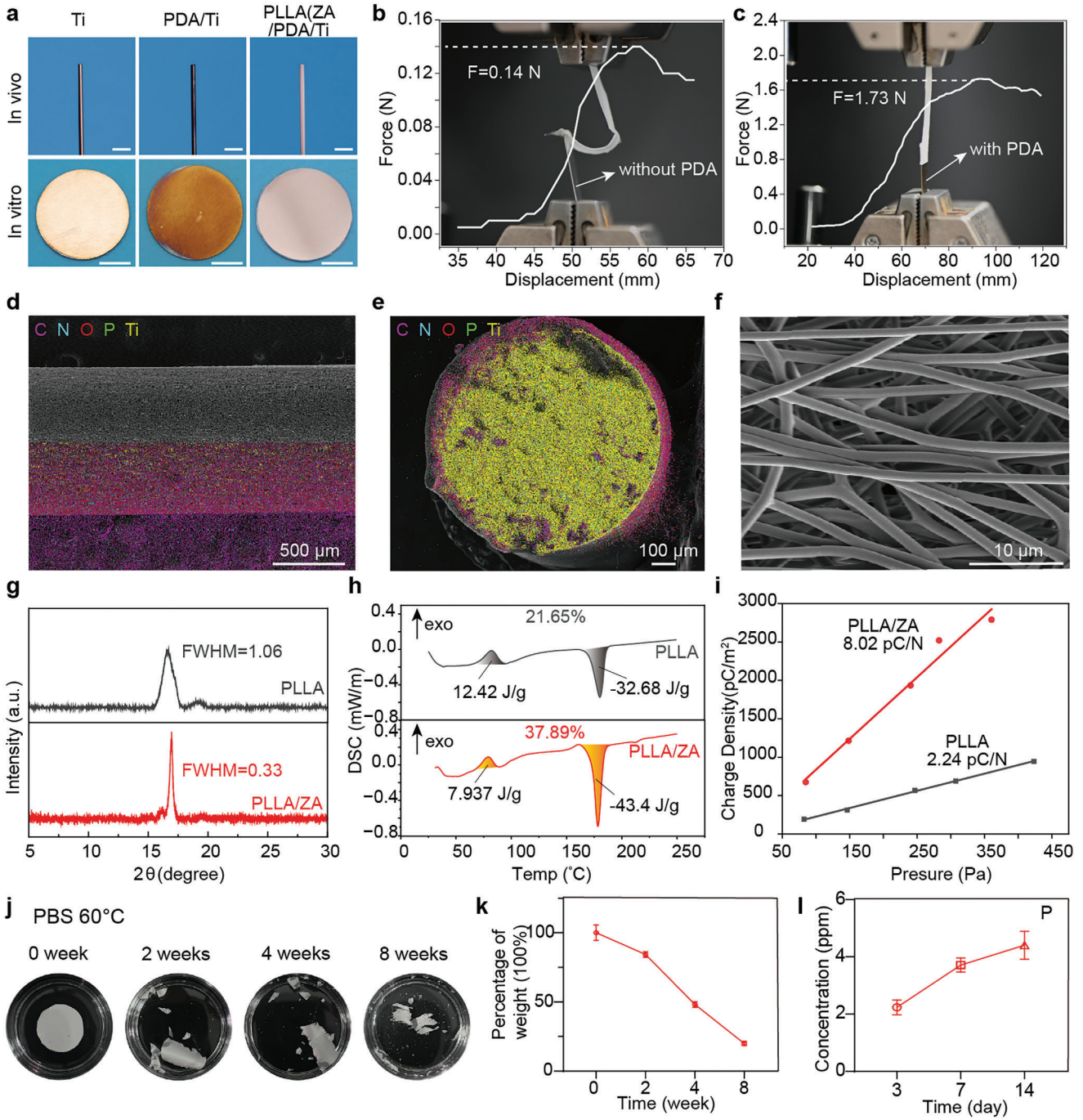

Figure 2. Preparation and characterization of piezoelectric PLLA/ZA coatings. a) For in vivo and in vitro experiments, physical pictures of the preparation process of the titanium surface coating. A layer of PDA was modified on the Ti surface first, and then PLLA/ZA coating was spun on the PDA. b,c) Force-displacement curves required for the coating to be stripped from the Ti surface with or without PDA. d,e) Side view and cross-section SEM images of Ti rods with PLLA/ZA coating and the mapping distribution of elements C, N, O, P, Ti, showing that ZA is uniformly dispersed in PLLA and the coating thickness is around 50 μm. f) Representative SEM image of PLLA/ZA coating. g) XRD analysis and h) DSC curves of PLLA and PLLA/ZA coating, the full-peak half-peak widths of the peaks in the α-phase ($2\theta = 16.7°$) are 1.06 and 0.33, respectively. (h) DSC curves of PLLA and PLLA/ZA, the crystallinity calculated from the curves are 21.65% and 37.89%, respectively. i) Piezoelectric coefficients in the d_{14} direction for PLLA (2.24 pC/N) and PLLA/ZA (8.02 pC/N). j) Images of the accelerated degradation process of PLLA/ZA coating and mass-time curve. k) Test of ZA release rate represented by P element.

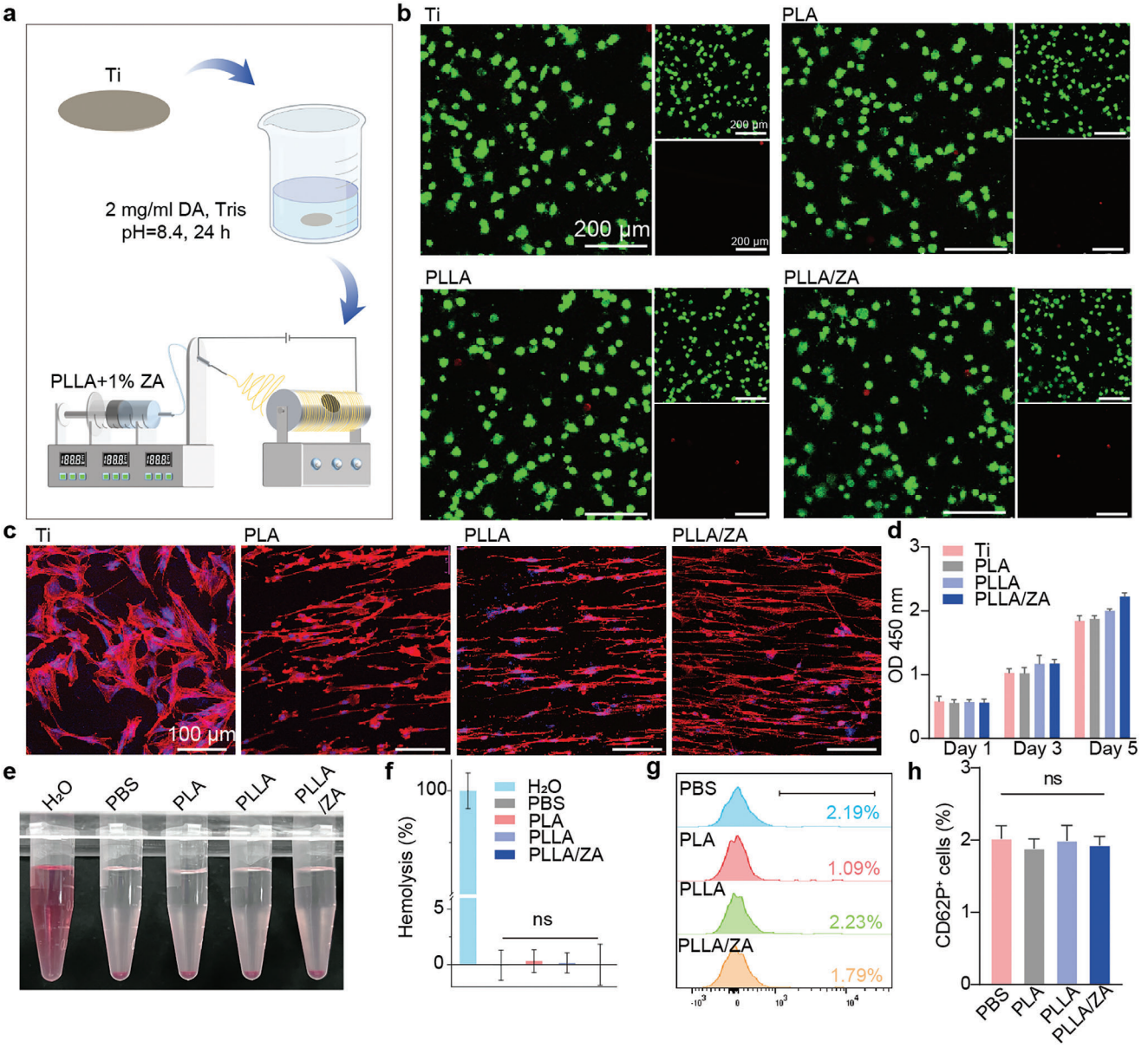

Figure 3. Biocompatibility testing of PLLA/ZA coatings. a) Schematic of the coating preparation process for in vitro experiments. b) Live-dead staining of MSCs grown on the surface of different materials groups for 24 h. c) Morphological staining of MSCs grown on the surface of different materials groups for 48 h. d) CCK8 test of MSCs grown on the different materials, which is proportional to cell viability. (n = 5) e,f) Optical photographs of hemolysis assay test of different materials and (f) statistics of the percentage of hemolysis. (n = 5) g,h) Platelet activation test of different materials with percentage of $CD62P^+$ cells and (h) corresponding statistics. (n = 3).

osseointegration (**Figure** 4a).[42] Alkaline phosphatase (ALP) is a protein expressed early in osteogenic differentiation, marking the beginning of differentiation.[43] Tissue culture plates (TCP) were used as the control group, MSCs were seeded on the surface of different materials, and ALP staining after changing the differentiation medium for 3 days. As shown in Figure 4b, all groups of MSCs expressed ALP, with the highest expression observed in PLLA/ZA group. Extracellular calcium deposition was used as a marker of advanced osteoblast differentiation. Alizarin red staining was performed on cells from each group on day 7 and 14 to determine osteoblast maturation. PLLA was found to significantly increase mineralization compared to PLA without piezoelectricity, with the highest alizarin red (ARS) levels observed in the PLLA/ZA group (Figure 4c). Semi-quantitative statistical results for ALP and ARS are presented in Figure S4 (Supporting Information). Furthermore, real-time fluorescence quantitative polymerase chain reaction (qPCR) was used to quantify the genes related to osteogenesis, such as ALP, Runx2, OCN, and Col I, on day 7 of differentiation. The results were consistent with the previous findings, confirming that the piezoelectricity of PLLA/ZA was enhanced and significantly promoted the osteogenic differentiation of MSCs without external intervention (Figure 4d).

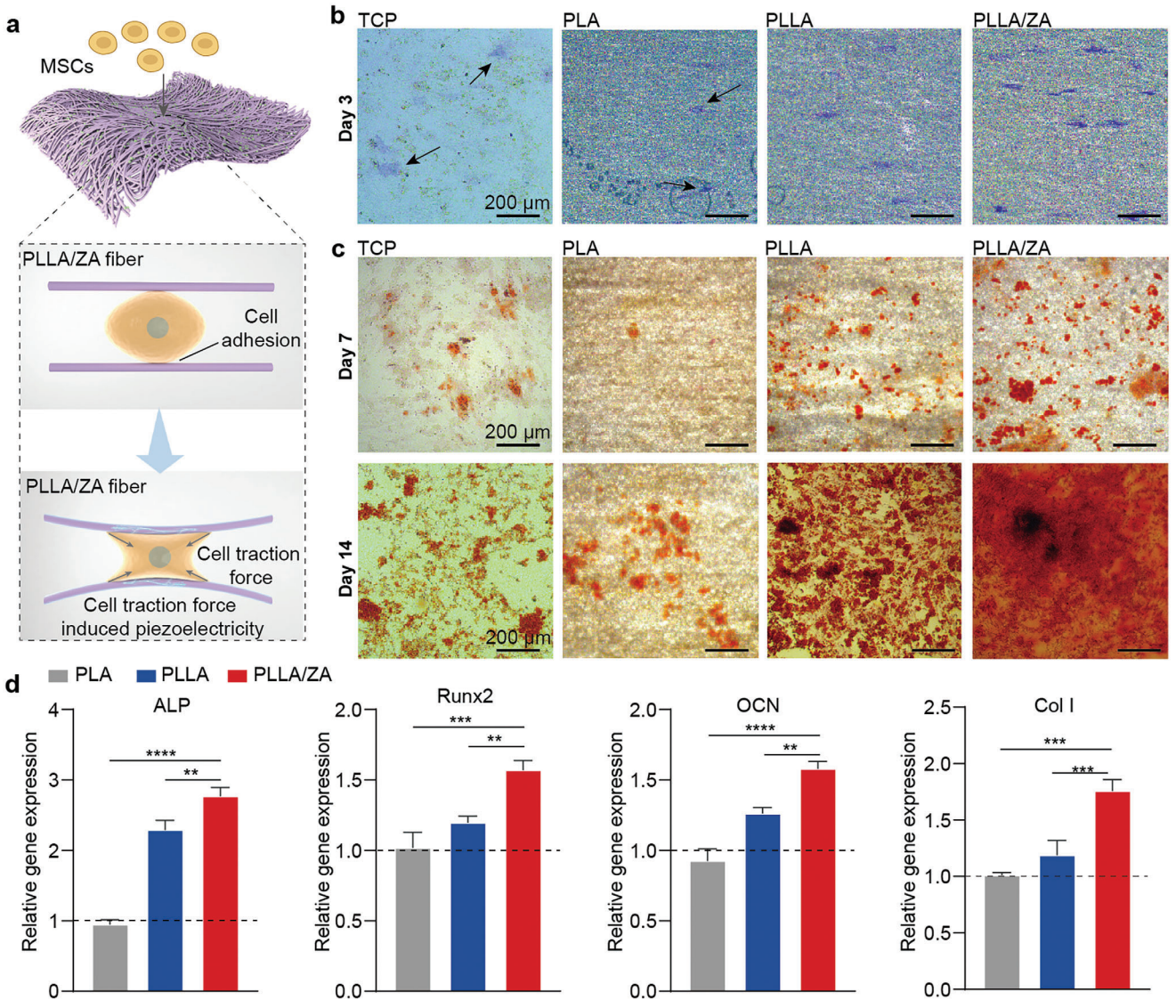

Figure 4. Effect of PLLA/ZA coating in vitro on osteogenic differentiation. a) Schematic diagram of the process of piezoelectricity generation by MSCs. b) ALP staining and c) Alizarin red staining of cells on the surface of TCP, PLA, PLLA and PLLA/ZA. (Day 3). c,d) Alizarin red staining of cells on the surface of TCP, PLA, PLLA and PLLA/ZA. (Day 7,14). (d) Relative expression of osteogenesis-related genes including ALP, Runx2, OCN and Col I in cells grown on the surface of PLA, PLLA and PLLA/ZA relative to TCP surface cells (Day 7).

2.4. The Effect of PLLA/ZA on Osteoclast Differentiation

Microscopic particles dislodged from implants are considered to be the primary cause of aseptic loosening of implants. Specifically, macrophages detach particles from the implant, which then undergo abnormal phagocytosis. This process produces cytokines and chemokines that lead to abnormal activation of osteoclasts and promote bone resorption, which resulting in aseptic loosening of the implant. The loosening of the implant, in turn, promotes the production of particles, leading to a vicious cycle. Therefore, inhibiting osteoclast activity and reducing bone resorption on the surface of bone implants is an effective means to break the cycle and prevent aseptic loosening.

ZA, a phosphate drug commonly used in the clinic for the treatment of osteoporosis, which effectively inhibits osteoclast function.[44] ZA dispersed in PLLA fibers is slowly released into the microenvironment surrounding the implant and further inhibits osteoclast differentiation by inhibiting the binding of RANKL to its receptor in bone marrow mononuclear macrophages (BMMs), which is the key signaling pathway for osteoclast differentiation (**Figure 5a**)[35]

Tartrate-resistant acid phosphatase (TRAP) was highly expressed in both osteoclast precursor cells and mature osteoclasts, making it an important marker for identifying the degree of osteoclastic differentiation.[45] As shown in Figure 5b, TRAP staining revealed that TRAP was expressed in all groups under osteoclastic differentiation-inducing medium. The control group expressed the highest amount of TRAP and showed mature fused multinucleated osteoclasts, which may be related to the stiffness of the substrate. Consistent with the anticipated results, there

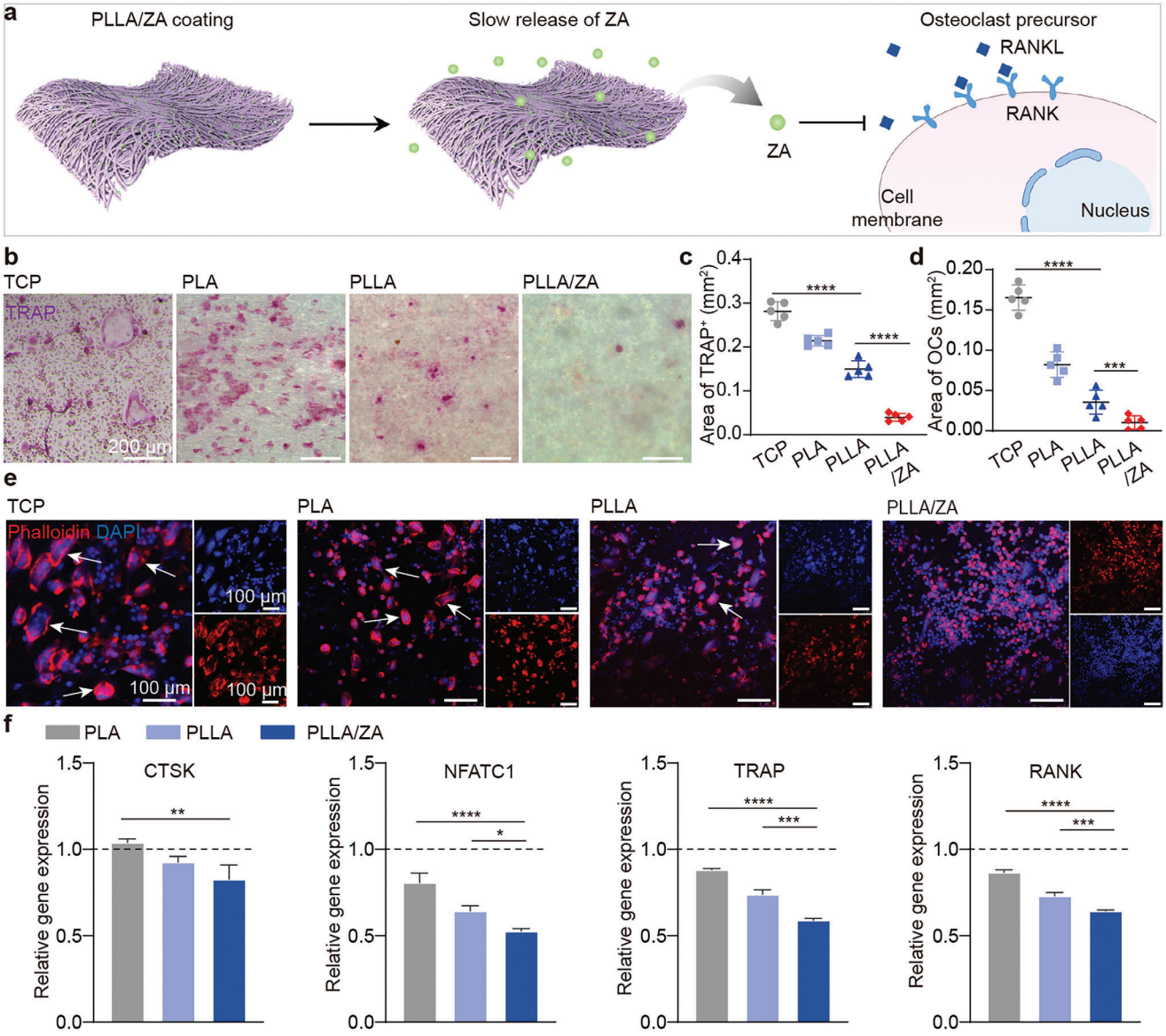

Figure 5. Effect of PLLA/ZA coating in vitro on osteoclast differentiation. a) Slow-releasing ZA from PLLA/ZA coating inhibits osteoclast differentiation by blocking the binding of RANKL and RANK. b) TRAP staining of BMMs after differentiation on TCP, PLA, PLLA and PLLA/ZA surfaces, purple areas are TRAP-positive areas and oval ring-shaped cells are mature osteoclasts (Day 4). c) Semi-quantitative statistics of $TRAP^+$ area per 1 mm^2 area in Figure 5b. d) Semi-quantitative statistics of the osteoclast area per 1 mm^2 in Figure 5e. e) Phalloidin (actin rings, red) and DAPI (nuclei, blue) staining of BMMs after differentiation on TCP, PLA, PLLA and PLLA/ZA surfaces, cells with more than 3 nuclei were defined as mature osteoclasts (Day 5). f) Relative expression of osteoclast-related genes including CTSK, NFATC1, TRAP and RANK in cells grown on the surface of PLA, PLLA and PLLA/ZA relative to that on TCP surface cells (Day 4).

were only a few TRAP-positive regions, indicating that PLLA/ZA significantly inhibited osteoclast differentiation. It is noteworthy that TRAP expression was also suppressed in the PLLA group compared to PLA without piezoelectricity, leading us to speculate that piezoelectricity influenced osteoclast differentiation. The expression area of TRAP was also quantitatively counted, as shown in Figure 5c, the area of TRAP expression in the PLLA/ZA group was the lowest, and the results were statistically significant.

Osteoclasts are multinucleated cells formed by the fusion of mononuclear macrophages. Mature osteoclasts are defined as those with three or more nuclei.[46] To assess their function, actin rings and nuclei were fluorescently stained, and the total area of mature osteoclasts was counted (Figure 5d). Figure 5e shows that mature osteoclasts have large elliptical actin rings and multiple nuclei, with almost no mature osteoclasts observed in the PLLA/ZA group. The results of qPCR showed that signature genes associated with osteoclasts including cathepsin K (CTSK), nuclear factor of activated T cells c1 (NFATC1), TRAP and RANK were significantly downregulated in the PLLA/ZA group (Figure 5f). These results suggested that PLLA/ZA could inhibit osteoclast differentiation through the dual effects of

piezoelectric and ZA, and ZA played a significant role in blocking the formation of osteoclasts almost completely.

2.5. In Vivo Rat Experiments

In order to verify the ability of PLLA/ZA coating for early osseointegration of Ti implants in practical applications, surgical implantation of Ti rods in the femoral bone cavity of rats was performed. Three experimental groups of Ti rods (Ti), Ti rods with modified PLLA coatings (Ti-PLLA), and Ti rods with modified PLLA/ZA coatings were established (Ti-PLLA/ZA), and a certain amount of Ti particles were injected into the bone cavity to simulate wear particles dislodged by the implant, and the specific surgical procedures are shown in Figure S5 (Supporting Information).[4]

Four weeks after implantation, rat femurs were sampled, and micro-CT analysis was performed to assess the osteogenesis around the Ti rods, i.e., the osseointegration of the implants, including the percentage of bone volume-to-tissue volume ratio (BV/TV), the number of trabeculae (Tb. N), and the degree of trabecular segregation (Tb. Sp). The PLLA/ZA coated Ti rods had the highest BV/TV of 75.06% at the same threshold and volume of interest on the CT scan (**Figure 6**a,c; Figure S6, Supporting Information). The region of interest of the PLLA/ZA coated group exhibited the highest number of Tb. N (Figure 6d) and the lowest Tb. Sp (Figure 6e), indicating an optimal osseointegration profile, which is consistent with the results of in vitro osteogenic differentiation experiments.

In order to study the specific details of the osseointegration around the implants, histological staining including hematoxylin-eosin (HE), Masson, toluidine blue and TRAP staining were performed. As shown in Figure 6b, new bone (blue staining) appeared around the implants, as seen in Masson staining of sections oriented perpendicular to and along the bone axis. The PLLA/ZA-coated Ti rods exhibited the largest and most continuous volume of new bone, as well as the greatest amount of new bone at the bone-implant junction, which visually demonstrates excellent osseointegration. HE staining and toluidine blue staining showed the same results (Figure S7, Supporting Information). To assess osteolysis around the implants, femoral cross sections near the implant were sectioned and stained for TRAP, with $TRAP^+$ area representing osteoclasts. In the PLLA/ZA-coated Ti rod group, there was almost no TRAP expression among the interconnected new bones; however, there was still TRAP expression in the bare Ti rod and PLLA-coated Ti rod groups (Figure 6g). In addition, the $TARP^+$ area was quantitatively counted in Figure 6f. In the final stage of the experiment, the vital organs (heart, liver, spleen, lung, kidney) of the rats in each group were sampled and stained in HE sections, and the results showed that there was no significant difference among the groups indicating the safety of the implanted materials (Figure S8, Supporting information).

Compared with the bare Ti rod group without Ti particles injection (Figure S9, Supporting Information), BV/TV was reduced from 46.72% to 11.67% in the group with Ti particles in the bone cavity, indicating successful induction of peri-implant osteolysis by Ti particles. Overall, the PLLA/ZA-coated Ti still had very good osseointegration ability under the challenge of Ti particles.

3. Conclusion

In conclusion, this study innovatively utilized ZA, as a nucleating agent for PLLA to successfully modify piezo-enhanced PLLA/ZA nanofibers on Ti surfaces. The deformation of PLLA/ZA fiber under cell traction force, leads to the generation of piezoelectric signals, which can effectively enhance osteoblast differentiation and bone formation. The sustained-release ZA from PLLA fibers can directly inhibit osteoclast differentiation and osteolysis. Both of them can facilitating the initiating of implants osseointegration, which is expected to reduce the occurrence of aseptic loosening and improve the long-term success rate of orthopedic surgery. Additionally, PLLA, as an FDA-approved implant material, has good biocompatibility and degradability. As a drug for the treatment of osteoporosis, ZA has been clinically safe and effective, indicating promising clinical application prospects. The strategy of combining material-based electrical stimulation with drug delivery can provide a valuable reference for surface modification of other bone implants.

4. Experimental Section

Fabrication of PLLA/ZA Piezoelectric Coatings: Piezoelectric spinning coatings were fabricated on the surface of Ti implants, where polydopamine was first modified on the Ti surface to enhance the bonding between the coating and Ti. For in vivo and in vitro experiments, different sizes of Ti were chosen, respectively, 14 mm diameter, 0.5 mm thick circular Ti sheets for cellular experiments and 1 mm diameter, 10 mm long cylindrical Ti rods for in vivo experiments. Ti was first immersed in the prepared aqua regia for 30 seconds to remove surface contaminants. Next, the Ti was immersed in a freshly configured 2 mg mL^{-1} dopamine-Tris solution (pH = 8.4) and kept in a shaker away from light for 24 h, which allowed the dopamine to polymerize and form a polydopamine (PDA) film on the Ti surface. Excess PDA remaining on the Ti surface was rinsed off with running water and then the Ti was allowed to dry naturally. The spinning solution was PLLA with a molecular weight of 300000 dissolved with stirring in hexafluoroisopropanol (aladdin) at a concentration of 10% for 2 h. The PLLA/ZA solution was based on the above with the addition of zoledronic acid (aladdin) at a mass fraction of 1% of PLLA. Specifically, for the cell experiments, Ti sheets were bonded to the surface of the drum receiver, the spinning parameters were positive high voltage of 10 kV, negative high voltage of -3 kV, receiver speed of 1800 r min^{-1}, spinning solution flow rate of 1 mL h^{-1} and total working time of 90 min. In contrast, Ti in the form of rods was fixed to a homemade high-speed rotating receiver directly connected to negative high pressure to achieve rapid enrichment of surface fibers with the working time of 5 min. The resulting spun coating was held at 120 °C for 4 h and cooled naturally for annealing, which was used to obtain the piezoelectricity of the polymer. In particular, the unannealed PLLA is called PLA, which was the group without piezoelectricity.

Characterization of Scaffold: The microstructure and elemental composition of the nanofibers was characterized by Nova 450 scanning electron microscope (SEM) and Raith/EDAX (EDS). XRD was performed with a PANalytical X'Pert3 diffractometer (PANalytical Ltd., Netherlands) loaded a Cu Kα source with a step of 0.013° and a 2θ range from 5° to 80°. FTIR spectra were obtained using a Vertex 80 V (Bruker Corp, MA, USA). The adhesion between the spun coating and Ti was tested by Mark 10. DSC curves were tested by TA Q200 under conditions of 10°C $minute^{-1}$ temperature increase from 25 to 250 °C. To assess the slow release rate of ZA, 10 mg of PLLA/ZA was submerged in 1 mL of deionized water at 37 °C, and the concentration of elemental P in the solution was assayed

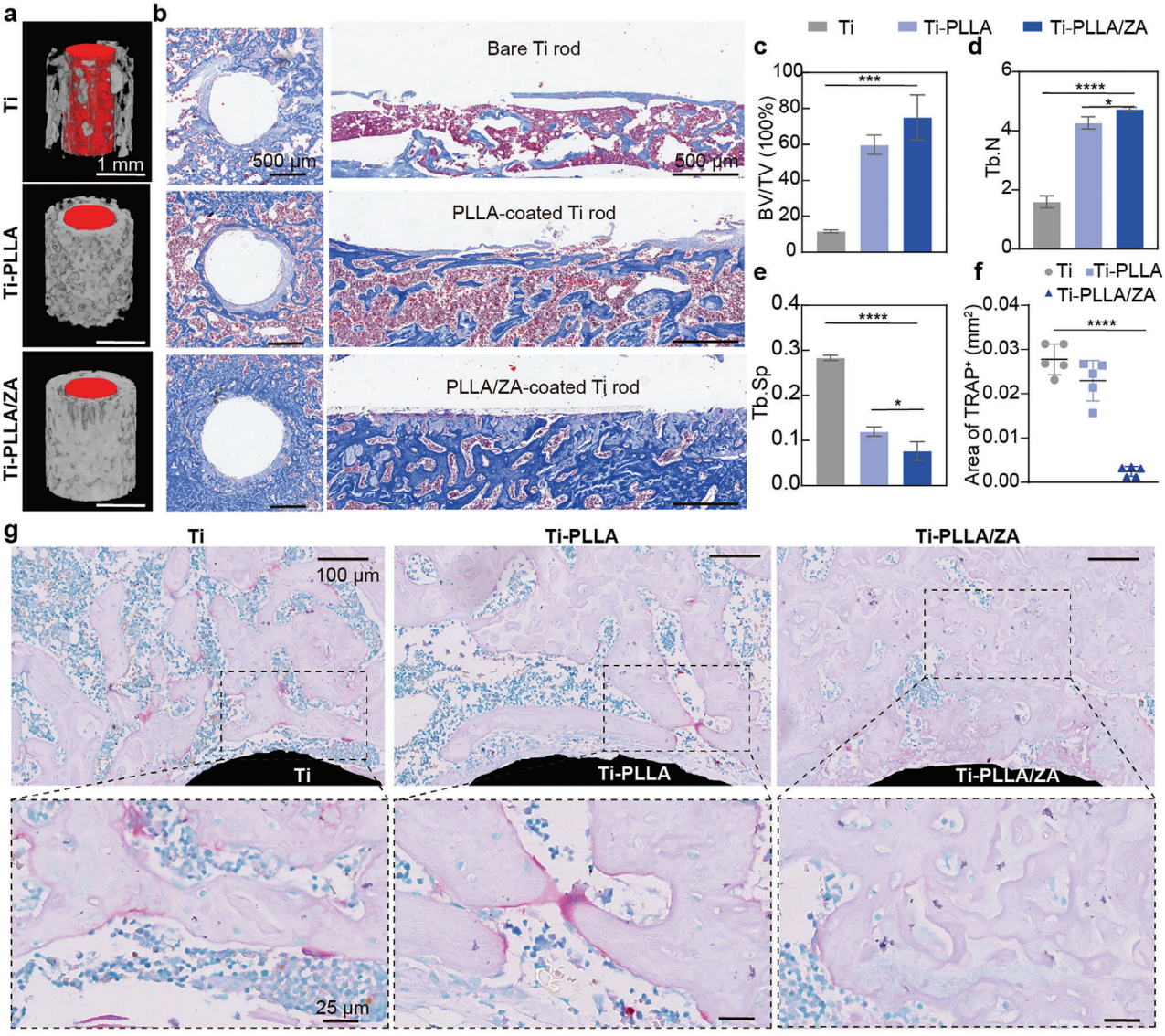

Figure 6. In vivo experiments on aseptic loosening of PLLA/ZA coatings on bone implants. a) CT images of new bone regeneration in the region of interest around implants 4 weeks after implantation. b) Masson staining of sections perpendicular to and along the long axis of the bone at uniform depth of the implant, with areas of new bone in dark blue. c) Bone volume to tissue volume (BV/TV) of new bone in the region of interest. d) Number of trabeculae of newborn bone in the region of interest. e) Trabecular separation (Tb.Sp) of the neonatal bone in the region of interest. f) Semiquantitative statistics of $TRAP^+$ area per 1 mm^2 area in Figure 5g. g) TRAP staining was performed on sections of the same depth perpendicular to the long axis of the bone, and local magnification of sections perpendicular to the long axis of the bone performed to the same depth of the implant; purple areas are TRAP-positive areas, representing active osteolysis.

on days 3, 7 and 14 using ThermoICPOES7200. The in vitro accelerated degradation experiments of PLLA/ZA thin film materials were realized in a PBS solution environment at 60 °C. Each 14 mm diameter film corresponded to 3 mL of PBS solution,c and the solution was changed every 3 days (n = 5).

Determination of d_{14} Piezoelectric Coefficient: In this study, the evaluation of the d_{14} piezoelectric coefficient for various films was conducted using an in-house developed testing apparatus specifically designed for d_{14} piezoelectric measurements. The process involved depositing a metallic silver layer onto each side of a thin film substrate, measuring 1 × 1 cm, through the process of magnetron sputtering. This deposition utilized a PVD75 Kurt J. Lesker system under an argon atmosphere at a pressure of 4 mTorr, employing a power setting of 100 W for a duration of 15 min. To assess the piezoelectric properties, a predetermined force was exerted on the film in alignment with the orientation of the fibers. This action facilitated the generation of piezoelectric responses from both surfaces of the film. The quantification of the d_{14} piezoelectric coefficient was achieved through the application of the subsequent formula:

$$d_{14} = \frac{D_{sur}}{T_4} = \frac{Q_{sur}}{A_{sur}} \left(\frac{F}{A_{cro}}\right)^{-1} = \frac{A_{cro}}{A_{sur}} \cdot \frac{\int Idt}{F} \quad (1)$$

herein, D_{sur} denotes the density of the surface charge, T_4 represents the stress applied in the direction of shear, Q_{sur} indicates the charge generated on the surface, A_{sur} refers to the area of the surface, F signifies the

force exerted, A_{cro} describes the cross-sectional area, *I* denotes the current produced, and *t* was the duration of the current flow.

Hemolysis Rate Testing: The material film was immersed in PBS at a ratio of 6 cm^2 mL^{-1} and kept at 37 °C for 1 h to obtain the material extract. Deionized water was used as positive control and PBS as negative control, and PLA, PLLA, PLLA/ZA were set up as experimental groups (n = 5). 2 mL of fresh rat blood was taken and diluted with 10 mL of PBS, 100 µL of diluted blood was added to each 1 mL of sample and kept at 37 °C for 60 min. The samples were centrifuged at 800 g for 5 min, the color depth of the supernatant was proportional to the haemolysis rate, the absorbance of the supernatant was measured at 545 nm with the enzyme marker and the absorbance at 655 nm was used as a reference, and the absorbance of the groups was calculated.

Assessment of Platelet Activation: Investigations into platelet activation were conducted by measuring the expression levels of the platelet activation marker P-Serotonin (CD62P) on the surface of platelets in vitro. Samples were immersed in PBS solution at 37 °C for a duration of 24 h to procure the extract. Blood was drawn via cardiac puncture from Sprague-Dawley rats. This extract was subsequently incubated with whole blood at ambient temperature for 30 min, in conjunction with specific antibodies: FITC-CD61 and PE-CD62P (sourced from BioLegend). Analysis of the cells through flow cytometry was performed thereafter, aiming to discern the extent of non-specific platelet activation.

Cell Viability and Morphology: Staining for dead and live cells: Samples were stained for dead and live cells according to the actual instructions (Calcein-AM/PI, Beijing Solarbio Science & Technology Co.) to determine the percentage of dead and live cells. Specifically, samples were digested with trypsin and resuspended in a staining solution after centrifugation and incubated in a cell culture incubator for 25 min. The sample cells were then mixed and added to a laser confocal plate and immediately observed by laser confocal (TCS SP8, Leica). Live cells were stained with green fluorescence, and dead cells were stained with red fluorescence.

Cell Proliferation and Cell Count Kit-8 (CCK-8): The supernatant medium of the samples was replaced with medium containing 10% CCK-8. Then, the samples were continued to be incubated in the cell culture incubator for 1 h, resulting in the upper layer of the medium turning to varying degrees of brown. The supernatant of 150 µL was pipetted from each sample placed in a 96-well plate immediately using an enzyme-labelled instrument to detect its absorbance at 450 nm, which is proportional to the viability of the cells.

Cell Morphology and Cytoskeleton Detection: Each specimen was preserved in a 4% solution of paraformaldehyde for a duration of 10 min at ambient temperature, followed by immersion in a permeabilization solution for 5 min at a temperature of 4 °C. Subsequent to this, the specimens underwent a series of washes using PBS buffer before being subjected to a 1-h incubation period at 37 °C with Rhodamine-Phalloidin (Abcam, diluted 1:1000). Following this incubation, the specimens were rinsed thrice with PBS buffer and then exposed to DAPI staining solution (4′,6-diamidino-2-phenylindole, Solarbio, at a dilution of 1:200) for 10 min at 37 °C. After a final set of washes in PBS, the specimens were mounted beneath glass coverslips in preparation for examination under a laser confocal microscope (TCS SP8, Leica).

Collection and Culture of Primary Mesenchymal Stem Cells (MSCs): MSCs were isolated from the cranial bone of neonatal Sprague-Dawley rats aged three days, following a meticulous surgical approach. The procedure began with euthanizing the rats, followed by sterilization of the cranial surface with alcohol, and then delicately removing the skull. The excised skull was then subjected to enzymatic dissociation using trypsin at a controlled temperature of 37 °C for a duration of 10 min. Following the trypsinization, the enzyme solution was discarded and replaced with collagenase I (1 mg mL^{-1} concentration) and incubated for an additional 30 min at 37 °C. Subsequently, the bone fragments were finely minced and incubated in a fresh batch of collagenase I solution for 60 min. The resulting supernatant was then centrifuged to sediment the MSCs, which were then harvested for further cultivation. For the expansion of MSCs, cells were propagated through generations 3 to 6 utilizing α-MEM medium (Gibco), which was enriched with 10% fetal bovine serum (Gibco) and 1% penicillin-streptomycin (Solarbio). To induce osteogenic differentiation, the culture medium was supplemented with dexamethasone (0.01 mmol L^{-1}), sodium β-glycerophosphate (10 mmol L^{-1}), and ascorbic acid (0.5 mmol L^{-1}) to the basal α-MEM medium. Cultivation took place in a humidified incubator set at 37 °C and a 5% CO_2 atmosphere, with the culture medium refreshed every two to three days.

Collection and Culture of Primary Bone Marrow Mononuclear Macrophages (BMMs): BMMs were isolated from the bone marrow of C57 mice according to surgical protocols.

Specifically, 6-8-week-old female C57 mice were decapitated and killed by immersion in 75% alcohol for 3 min before being sorted for tibia and femur in a clean table. The ends of the bones were cut then the bone marrow was blown out with PBS, which were lysed for 3 min in a cleavage red solution. After centrifugation, the precipitate was resuspended in α-MEM medium and seeded for plate culture. In general, three mice corresponded to one 10 cm diameter cell culture dish. After 12 h, the supernatant was collected and centrifuged and the precipitate was resuspended by α-MEM medium containing 50 ng/mL M-CSF (Peprotech) and seeded for a new plate. After three days, the supernatant in the plate was discarded and the cells were washed three times with PBS and then scraped off in PBS by cell scraping which were to be BMMs. Osteoclast differentiation medium supplemented with 50 ng mL^{-1} M-CSF and 100 ng/mL RANKL (Peprotech). The incubator was set at 37 °C with 5% CO_2 and the cell culture medium is changed every 2 to 3 days. Cells were plated at a density of 2×10^4 cm^{-2} and mature osteoclasts appeared on day 4 after the use of differentiation medium.

Staining for Characteristic Cellular Proteins: *ALP Staining*: Cell samples were fixed in 4% paraformaldehyde for 10 min, then rinsed 3 times with PBS and incubated with the ALP incubation solution for 25 min at 37 °C according to the reagent manufacturer's instructions (Solarbio), and then observed under a leica inverted microscope after washing with PBS. The blue-violet area indicated ALP protein expression, which is indicative of osteoblast differentiation.

Alizarin Red Staining: Cell samples were fixed in 4% paraformaldehyde for 10 min, then rinsed 3 times with PBS, incubated with alizarin red incubation solution for 30 min at room temperature, and observed under a metallurgical microscope after washing with PBS, the calcium nodules were stained with red color, which was correlated with the degree of mineralization of osteoblasts.

TRAP Staining: osteoblast samples were fixed in 4% paraformaldehyde for 10 min, then washed three times with PBS, TRAP incubation solution (Solarbio) was incubated at 37 °C for 30 min, and the osteoblast progenitor cells and mature osteoblasts were stained with purple-red color, and the mature osteoblasts appeared in the form of an irregular circle.

Quantitative Real-Time Polymerase Chain Reaction Analysis(qPCR): RNA extraction was performed on cellular samples utilizing the RC112-01 (FastPure Cell/Tissue Total RNA Isolation Kit V2, Vazyme Biotech Co., Ltd) kit, strictly following the supplier's protocol. The RNA yield was quantitatively assessed using a nanodrop technique. For reverse transcription, a reaction mixture was constituted comprising 1000 ng of RNA, 4 µL of 5 × RT Master Mix, and RNase-free water to a final volume of 20 µL. This mixture was thoroughly homogenized and then subjected to a PCR amplification process under specified thermal cycling conditions: an initial phase at 37 °C for 30 min, followed by a denaturation step at 85 °C for 1 min, and a final hold at 4 °C. Subsequent to reverse transcription, the cDNA was diluted to a working concentration of 2.5 ng μL^{-1}. qPCR setup was prepared according to the protocol provided for the R323-01 SYBR Green reagent, comprising 5 µL of SYBR Green, 0.4 µL of both forward and reverse primers, 2 µL of the prepared cDNA, and RNase-free water to adjust the total volume to 10 µL. This qPCR reaction mixture was adequately mixed and allocated into the PCR system to undergo thermal cycling as follows: an initial step at 37 °C for 15 min, followed by a rapid heat to 85 °C for 5 seconds. The CT values were determined and gene expression analysis was conducted utilizing the ΔΔCT method.

Animals and Surgical Procedures: Female Sprague-Dawley rats, each weighing ≈ 220g and aged between 6 to 8 weeks, were acquired from Vital River Company, located in Beijing, China. The conduct of all experiments involving these animals was strictly in line with the ethical guidelines set forth by the Ethics Committee of the Beijing Institute of Nanoenergy and

Nanosystems. To ensure the highest standards of sterility, all surgical procedures were carried out in a meticulously sanitized environment, with all surgical tools subjected to autoclaving prior to their use in surgeries. Specifically, as shown in Figure S5 (Supporting Information), a 1 mm diameter hole was drilled at the femoral joint in the direction of the bone axis, and the bone cavity was injected with 100 µL of a 40% PBS dispersion of Ti nanoparticles. A 1 cm Ti rod implant was inserted into the bone cavity, the wound was sutured and antibiotics were injected.

Micro-Computed Tomography Scanning Evaluation: At 4 weeks after implantation, the rats were euthanized and the femurs were removed and fixed in formalin for 24 h. The micro-CT with a scanning accuracy of 12 µm was used to scan the femurs at a voltage of 100 kV and a current of 85 µA. As shown in Figure S6(Supporting Information), the region of interest, also known as the circular column region, was analyzed for bone volume / tissue volume (BV/TV), trabecular number (Tb. N) and trabecular density (Tb. Sp) at a depth of 2 mm to 4 mm below the bone plate and a thickness of 0.5 mm around the implant.

Histological Analysis: The femur was sectioned after 4 weeks of decalcification. To assess the osseointegration around the implants, the femur as well as the vital organs were sectioned and analyzed with histological stains, including HE, Masson, Toluidine blue and, TARP analysis.

Statistical Evaluation: The results were presented as the mean ± standard deviation. Differences among the groups were assessed using one-way analysis of variance (ANOVA) to determine statistical significance. A threshold of $p < 0.05$ was considered indicative of significant differences (**** for $p < 0.0001$, *** for $p < 0.001$, ** for $p < 0.01$, * for $p < 0.05$).

Availability of Data: The datasets underpinning the conclusions drawn in this study were comprehensively included within the main article, Supplementary Materials, and the dedicated Source data file. The complete set of image data can be made available by the corresponding author upon formal request. Additionally, source data accompanying this publication are openly provided.

Supporting Information

Supporting Information is available from the Wiley Online Library or from the author.

Acknowledgements

This work was financially supported by Beijing Natural Science Foundation (L212010), The Scientific Research Project of Suzhou Gusu Medical Talents Program (GSWS2022041), Scientific research project of Jiangsu Provincial Health Commission (H2023139), and The Fundamental Research Funds for the Central Universities.

Conflict of Interest

The authors declare no conflict of interest.

Author Contributions

L.X., Y Z., M Z. and Z.L. were responsible for the experimental concept and design. X.C., Y.S., and J.L. designed the study. X.C., J.L., M.X., J.J., E.W. performed experimental measurement and data analyses. X.C., Y.S., M.X., B.Z. took and processed the experimental photograph. X.C. wrote the original draft. L.X., Y.Z., M.Z., and Z.L. were responsible for project administration, conceptualization, supervision, funding acquisition, validation and review. All authors discussed the results and commented on the manuscript.

Data Availability Statement

The data that support the findings of this study are available from the corresponding author upon reasonable request.

Keywords

aseptic loosening, nucleating agent, piezoelectric, PLLA, zoledronic acid

Received: March 1, 2024
Revised: April 30, 2024
Published online:

[1] N. A. Hodges, E. M. Sussman, J. P. Stegemann, *Biomaterials* **2021**, *278*, 121127.
[2] Y. Abu-Amer, I. Darwech, J. C. Clohisy, *Arthrit. Res. Ther.* **2007**, *9*, Suppl1.
[3] Z. Liu, X. Wan, Z. Wang, L. Li, *Adv. Mater.* **2021**, *33*, 32.
[4] T. D. Zaveri, N. V. Dolgova, J. S. Lewis, K. Hamaker, M. J. Clare-Salzler, B. G. Keselowsky, *Biomaterials* **2017**, *115*, 128.
[5] N. C. Liu, J. Meng, Z. H. Wang, G. Zhou, T. G. Shi, J. N. Zhao, *Biochem. Biophys. Res. Commun.* **2016**, *473*, 133.
[6] P. Drees, A. Eckardt, R. E. Gay, S. Gay, L. C. Huber, *Nat. Clin. Pract. Rheumatol.* **2007**, *3*, 165.
[7] H. Cui, W. Wang, L. Shi, W. Song, S. Wang, *Small Methods* **2020**, *4*, 2000573.
[8] S. B. Goodman, Z. Y. Yao, M. Keeney, F. Yang, *Biomaterials* **2013**, *34*, 3174.
[9] K. Li, Z. Tang, K. Y. Song, N. G. Fischer, H. H. Wang, Y. L. Guan, Y. Y. Deng, H. Cai, S. Ul Hassan, Z. Ye, T. Sang, *Colloid Surf. B-Biointerfaces* **2023**, *232*, 113604.
[10] Y. Zhang, J. S. Cui, K. Y. Chen, S. H. Kuo, J. Sharma, R. Bhatta, Z. Liu, A. Ellis-Mohr, F. F. An, J. H. Li, Q. Chen, K. D. Foss, H. Wang, Y. M. Li, A. M. McCoy, G. W. Lau, Q. Cao, *Sci. Adv.* **2023**, *9*, 18.
[11] Y. Yin, Q. L. Huang, M. H. Yang, J. Xiao, H. Wu, Y. Liu, Q. X. Li, W. D. Huang, G. H. Lei, K. Zhou, *ACS Biomater. Sci. Eng.* **2020**, *6*, 3005.
[12] Z. Liu, Q. Tang, R. T. Liu, M. Z. Yu, H. Peng, C. Q. Zhang, Z. Z. Zhu, X. J. Wei, *Bioact. Mater.* **2023**, *22*, 60.
[13] Y. J. Wei, Z. Q. Liu, X. Zhu, L. Jiang, W. D. Shi, Y. J. Wang, N. Xu, F. L. Gang, X. M. Wang, L. Y. Zhao, J. Lin, X. D. Sun, *Biomaterials* **2020**, *257*, 120237.
[14] M. F. Yu, D. Q. You, J. J. Zhuang, S. Y. Lin, L. Q. Dong, S. T. Weng, B. Zhang, K. Cheng, W. J. Weng, H. M. Wang, *ACS Appl. Mater. Interfaces* **2017**, *9*, 19698.
[15] M. Djosic, A. Jankovic, V. Miskovic-Stankovic, *Materials* **2021**, *14*, 18.
[16] N. J. Shah, M. N. Hyder, J. S. Moskowitz, M. A. Quadir, S. W. Morton, H. J. Seeherman, R. F. Padera, M. Spector, P. T. Hammond, *Sci. Transl. Med.* **2013**, *5*, 191.
[17] V. Zarghami, M. Ghorbani, K. P. Bagheri, M. A. Shokrgozar, *Prog. Org. Coat.* **2020**, *139*, 105440.
[18] Y. C. Shi, L. T. Wang, Y. M. Niu, N. Yu, P. F. Xing, L. Dong, C. M. Wang, *Adv. Funct. Mater.* **2018**, *28*, 1804483.
[19] R. Agarwal, A. J. García, *Adv. Drug Del. Rev.* **2015**, *94*, 53.
[20] S. Zhu, Y. Tang, C. Lin, X. Y. Liu, Y. Lin, *Small Methods* **2021**, *5*, 2001060.
[21] Y. Kong, J. Z. Duan, F. Liu, L. Han, G. Li, C. H. Sun, Y. H. Sang, S. H. Wang, F. Yi, H. Liu, *Chem. Soc. Rev.* **2021**, *50*, 12828.
[22] G. L. Koons, M. Diba, A. G. Mikos, *Nat. Rev. Mater.* **2020**, *5*, 584.
[23] R. Z. Luo, Y. Liang, J. R. Yang, H. Q. Feng, Y. Chen, X. P. Jiang, Z. Zhang, J. Liu, Y. Bai, J. T. Xue, S. Y. Chao, Y. Xi, X. Q. Liu, E. G. Wang, D. Luo, Z. Li, J. P. Zhang, *Adv. Mater.* **2023**, *35*, 2208395.
[24] Y. Z. Zhang, L. L. Xu, Z. Liu, X. Cui, Z. Xiang, J. Y. Bai, D. J. Jiang, J. T. Xue, C. Wang, Y. X. Lin, Z. Li, Y. Z. Shan, Y. Yang, L. Bo, Z. Li, X. Z. Zhou, *Nano Energy* **2021**, *85*, 106009.
[25] M. A. Fernandez-Yague, A. Trotier, S. Demir, S. A. Abbah, A. Larrañaga, A. Thirumaran, A. Stapleton, S. A. M. Tofail, M. Palma, M. Kilcoyne, A. Pandit, M. J. Biggs, *Adv. Mater.* **2021**, *33*, 2008788.

[26] S. Singh, E. L. Nyberg, A. N. O'Sullivan, A. Farris, A. N. Rindone, N. Zhang, E. C. Whitehead, Y. Zhou, E. Mihaly, C. C. Achebe, W. Zbijewski, W. Grundy, D. Garlick, N. D. Jackson, T. Taguchi, C. Takawira, J. Lopez, M. J. Lopez, M. P. Grant, W. L. Grayson, *Biomaterials* **2022**, *282*, 121392.
[27] T. Wang, H. Ouyang, Y. Luo, J. Xue, E. Wang, L. Zhang, Z. Zhou, Z. Liu, X. Li, S. Tan, Y. Chen, L. Nan, W. Cao, Z. Li, F. Chen, L. Zheng, *Sci. Adv.* **2024**, *10*, eadi6799.
[28] B. Yu, Z. G. Qiao, J. J. Cui, M. F. Lian, Y. Han, X. Zhang, W. Q. Wang, X. G. Yu, H. Yu, X. D. Wang, K. L. Lin, *Biomaterials* **2021**, *276*, 120997.
[29] T. Vinikoor, G. K. Dzidotor, T. T. Le, Y. Liu, H. M. Kan, S. Barui, M. T. Chorsi, E. J. Curry, E. Reinhardt, H. Z. Wang, P. Singh, M. A. Merriman, E. D'Orio, J. Park, S. Y. Xiao, J. H. Chapman, F. Lin, C. S. Truong, S. Prasadh, L. Chuba, S. Killoh, S. W. Lee, Q. Wu, R. M. Chidambaram, K. W. H. Lo, C. T. Laurencin, T. D. Nguyen, *Nat. Commun.* **2023**, *14*, 6257.
[30] Y. Liu, G. Dzidotor, T. T. Le, T. Vinikoor, K. Morgan, E. J. Curry, R. Das, A. McClinton, E. Eisenberg, L. N. Apuzzo, K. T. M. Tran, P. Prasad, T. J. Flanagan, S. W. Lee, H. M. Kan, M. T. Chorsi, K. W. H. Lo, C. T. Laurencin, T. D. Nguyen, *Sci. Transl. Med.* **2022**, *14*, 627.
[31] M. Vukomanovic, L. Gazvoda, M. Kurtjak, M. Macek-Krzmanc, M. Spreitzer, Q. Tang, J. Wu, H. Ye, X. Chen, M. Mattera, J. Puigmarti-Luis, S. V. Pane, *Small* **2023**, *19*, 2301981.
[32] Z. R. Liu, M. J. Cai, X. D. Zhang, X. Yu, S. Wang, X. Y. Wan, Z. L. Wang, L. L. Li, *Adv. Mater.* **2021**, *33*, 2106317.
[33] Y. Y. Tai, S. Yang, S. Yu, A. Banerjee, N. V. Myung, J. Nam, *Nano Energy* **2021**, *89*, 106444.
[34] C. J. Shuai, J. Zan, F. W. Qi, G. Y. Wang, Z. Liu, Y. W. Yang, S. P. Peng, *Mater. Des.* **2019**, *174*, 107801.
[35] D. B. Raina, L. M. Matuszewski, C. Vater, J. Bolte, H. Isaksson, L. Lidgren, M. Tägil, S. Zwingenberger, *Sci. Adv.* **2020**, *6*, 48.
[36] Y. Z. Li, L. Yang, Y. Hou, Z. Z. Zhang, M. Chen, M. X. Wang, J. Liu, J. Wang, Z. H. Zhao, C. M. Xie, X. Lu, *Bioact. Mater.* **2022**, *18*, 213.
[37] N. Jiang, Z. J. Guo, D. Sun, Y. B. Li, Y. T. Yang, C. Chen, L. Zhang, S. S. Zhu, *ACS Nano* **2018**, *12*, 7883.
[38] F. Y. Jiang, Y. Z. Shan, J. Y. Tian, L. L. Xu, C. H. Li, F. Yu, X. Cui, C. W. Wang, Z. Li, K. L. Ren, *Adv. Mater. Interfaces* **2023**, *10*, 2202474.
[39] Z. Shao, X. Zhang, J. Liu, X. Liu, C. Zhang, *Small Methods* **2023**, *7*, 2300701.
[40] G. Murillo, A. Blanquer, C. Vargas-Estevez, L. Barrios, E. Ibáñez, C. Nogués, J. Esteve, *Adv. Mater.* **2017**, *29*, 1605048.
[41] M. Kitsara, A. Blanquer, G. Murillo, V. Humblot, S. De Braganca Vieira, C. Nogues, E. Ibanez, J. Esteve, L. Barrios, *Nanoscale* **2019**, *11*, 8906.
[42] Z. R. Liu, J. H. Nie, B. Miao, J. D. Li, Y. B. Cui, S. Wang, X. D. Zhang, G. R. Zhao, Y. B. Deng, Y. H. Wu, Z. Li, L. L. Li, Z. L. Wang, *Adv. Mater.* **2019**, *31*, 1807795.
[43] J. J. Tian, R. Shi, Z. Liu, H. Ouyang, M. Yu, C. C. Zhao, Y. Zou, D. J. Jiang, J. S. Zhang, Z. Li, *Nano Energy* **2019**, *59*, 705.
[44] K. Kimachi, H. Kajiya, S. Nakayama, T. Ikebe, K. Okabe, *Naunyn-Schmiedeberg's Arch. Pharmacol.* **2011**, *383*, 297.
[45] B. Yuan, L. N. Wang, R. Zhao, X. Yang, X. Yang, X. D. Zhu, L. M. Liu, K. Zhang, Y. M. Song, X. D. Zhang, *Sci. Adv.* **2020**, *6*, 50.
[46] Y. Sun, J. B. Li, X. P. Xie, F. Gu, Z. J. Sui, K. Zhang, T. C. Yu, *Front. Cell. Dev. Biol.* **2021**, *9*, 788680.